

The functional small RNA interactome reveals targets for the vancomycin-responsive sRNA RsaOI in vancomycin-tolerant *Staphylococcus aureus*

Winton Wu,¹ Chi Nam Ignatius Pang,² Daniel G. Mediati,¹ Jai Justin Tree¹

AUTHOR AFFILIATIONS See affiliation list on p. 18.

ABSTRACT Small RNAs have been found to control a broad range of bacterial phenotypes including tolerance to antibiotics. Vancomycin tolerance in multidrug resistance *Staphylococcus aureus* is correlated with dysregulation of small RNAs although their contribution to antibiotic tolerance is poorly understood. RNA-RNA interactome profiling techniques are expanding our understanding of sRNA-mRNA interactions in bacteria; however, determining the function of these interactions for hundreds of sRNA-mRNA pairs is a major challenge. At steady-state, protein and mRNA abundances are often highly correlated and lower than expected protein abundance may indicate translational repression of an mRNA. To identify sRNA-mRNA interactions that regulate mRNA translation, we examined the correlation between gene transcript abundance, ribosome occupancy, and protein levels. We used the machine learning technique self-organizing maps (SOMs) to cluster genes with similar transcription and translation patterns and identified a cluster of mRNAs that appeared to be post-transcriptionally repressed. By integrating our clustering with sRNA-mRNA interactome data generated in vancomycin-tolerant *S. aureus* by RNase III-CLASH, we identified sRNAs that may be mediating translational repression. We have confirmed sRNA-dependant post-transcriptional repression of several mRNAs in this cluster. Two of these interactions are mediated by RsaOI, a sRNA that is highly upregulated by vancomycin. We demonstrate the regulation of HPr and the cell-wall autolysin Atl. These findings suggest that RsaOI coordinates carbon metabolism and cell wall turnover during vancomycin treatment.

IMPORTANCE The emergence of multidrug-resistant *Staphylococcus aureus* (MRSA) is a major public health concern. Current treatment is dependent on the efficacy of last-line antibiotics like vancomycin. The most common cause of vancomycin treatment failure is strains with intermediate resistance or tolerance that arise through the acquisition of a diverse repertoire of point mutations. These strains have been shown to altered small RNA (sRNA) expression in response to antibiotic treatment. Here, we have used a technique termed RNase III-CLASH to capture sRNA interactions with their target mRNAs. To understand the function of these interactions, we have looked at RNA and protein abundance for mRNAs targeted by sRNAs. Messenger RNA and protein levels are generally well correlated and we use deviations from this correlation to infer post-transcriptional regulation and the function of individual sRNA-mRNA interactions. Using this approach we identify mRNA targets of the vancomycin-induced sRNA, RsaOI, that are repressed at the translational level. We find that RsaOI represses the cell wall autolysis Atl and carbon transporter HPr suggestion a link between vancomycin treatment and suppression of cell wall turnover and carbon metabolism.

KEYWORDS small RNA, antibiotic resistance, MRSA, gene regulation

Editor Chris Greening, Monash University, Melbourne, Victoria, Australia

Address correspondence to Jai Justin Tree, j.tree@unsw.edu.au.

The authors declare no conflict of interest.

See the funding table on p. 18.

Received 11 September 2023

Accepted 11 March 2024

Published 27 March 2024

Copyright © 2024 Wu et al. This is an open-access article distributed under the terms of the [Creative Commons Attribution 4.0 International license](https://creativecommons.org/licenses/by/4.0/).

The emergence of multidrug-resistant *Staphylococcus aureus* (MRSA) is a major public health concern. Current treatment is dependent on the efficacy of last-line antibiotics like vancomycin. However, MRSA isolates that exhibit intermediate resistance (MIC 4–8 µg/mL) to vancomycin are increasingly detected worldwide and are associated with treatment failure (1). These vancomycin-intermediate *S. aureus* (VISA) isolates arise from the acquisition of a disparate series of point mutations that lead to physiological changes including cell wall thickening and reduced autolysis (2).

Transcriptional profiling has revealed that antibiotic treatment drives conserved changes in small RNA (sRNA) expression in *S. aureus* and may contribute to the VISA phenotype (3). Small RNAs have been established as global post-transcriptional regulators of bacterial gene expression which modulate mRNA expression by direct base-pairing. Small RNAs have been found to act by a wide array of mechanisms and have been shown to occlude the ribosomal binding site (4), activate translation (5), recruit and occlude RNase recognition (6, 7), control transcription termination (8), and modulate ribosome sliding to affect translation (9). In addition, sponging and buffering interactions (10–12) with other non-coding RNAs expand individual sRNA networks across multiple regulatory nodes.

Recent progress using proximity-dependant ligation techniques such as CLASH, RIL-seq, iRIL-seq, and Hi-GRIL-seq have massively expanded the number of sRNA-mRNA interactions identified *in vivo* (13–18). Using a technique termed CLASH (crosslinking, ligation, and sequencing of hybrids), sRNA-RNA interactions associated with the endoribonuclease RNase III were captured and sequenced in the MRSA strains JKD6009 and USA300 (12, 17). This was the first *in vivo* map of RNA-RNA interactions in a Gram-positive bacterium and revealed a regulatory mRNA 3' UTR that was required for vancomycin tolerance (17). In parallel work, small RNA regulation of the alpha phenol soluble modulins was uncovered (12).

RNA-RNA interaction networks identify interacting RNA pairs but do not provide information on the function of the interaction. Follow-up studies on individual sRNA-mRNA interactions are required to determine the regulatory functions and biological significance of the interaction. These studies typically employ RNA-seq or proteomics to monitor changes in transcript or protein abundance after the expression of a single sRNA and are not well suited to defining the functions of many different sRNAs on their cognate targets. These follow-up studies have also indicated that some sRNA-mRNA interactions recovered by *in vivo* proximity-dependant ligation do not affect mRNA transcript or protein abundance (14, 19). It is clear that for sRNA-RNA interaction networks recovered by proximity-dependant ligation, predicting the functional outcome of the interaction will require new approaches to determine system-wide sRNA-mRNA functions.

Here, we have captured the RNase III-associated RNA-RNA interactome of the VISA strain JKD6008. To identify mRNAs that are post-transcriptionally regulated, we have analyzed RNA-seq, Ribo-seq, and proteomics data to assess the correlation between mRNA abundance, translation, and protein abundance. Using this data, we have divided mRNAs into clusters using self-organising maps (SOMs) and overlaid these clusters with mRNAs interacting with sRNAs in our RNase III-CLASH network. SOMs were chosen for this analysis as it has an iterative refinement step and the analysis can be visualized as a two-dimensional map (20–22). This approach has been used by a few studies to cluster and visualize gene expression data in *Drosophila melanogaster*, *Caenorhabditis elegans*, various cancer cell lines, and crop plants (22–27). In bacteria, SOMs have been used for taxonomic classification of metagenomes and detection of horizontally transferred genes (28, 29). Using SOMs, we identified a cluster of mRNAs with below average correlation between mRNA and protein abundance that is enriched for sRNA-targeted mRNAs suggesting that sRNA regulation is responsible for the translational silencing of these mRNAs. We confirm that this SOMs cluster contains translationally repressed sRNA targets by examining the vancomycin-induced sRNA, RsaOI. We identify functional targets for RsaOI that are translationally repressed and promote mRNA turnover in our

SOMs clusters. The RsaOI targetome includes the autolysin *atl* that is involved in cell wall turnover and provides a pathway for post-transcriptional control of cell wall autolysis in response to vancomycin treatment.

MATERIALS AND METHODS

Bacterial strains and culture conditions

Bacterial strains and plasmids used in this study are listed in Table S1, while the oligonucleotides are listed in Table S2. *Escherichia coli* strains DH5 α and IMO8B were routinely cultured at 37°C in Luria-Bertani (LB) media. To facilitate plasmid maintenance in *E. coli*, LB media was supplemented with the following antibiotic concentrations when appropriate: 10 μ g/mL chloramphenicol or 100 μ g/mL ampicillin. On the other hand, *S. aureus* strains JKD6008 and JKD6009 were routinely cultured at 37°C in either Brain Heart Infusion media or Mueller-Hinton (MH) media. To facilitate plasmid selection in *S. aureus*, media were supplemented with the following antibiotic concentrations when appropriate: 10 μ g/mL chloramphenicol and/or 10 μ g/mL erythromycin. Construction of the RNase III-HTF tagged and deletion of RsaOI in *S. aureus* strain JKD6008 was performed through allelic exchange using the pIMAY-Z vector (30).

RNase III-CLASH of vancomycin-intermediate *S. aureus*

Preparation of the VISA RNase III-CLASH libraries was performed as outlined in our previous report (12, 17) with some modifications. *S. aureus* JKD6008 wild type, untreated JKD6008 RNase III-HTF, and vancomycin treated (final concentration of 2 μ g/mL for 10 min) JKD6008 RNase III-HTF cultures were grown in duplicates to an OD₆₀₀ of 0.8 in MH media. Cultures were crosslinked with 400 mJ of UV - C (Vari-X-Link, UV03) and immediately harvested by vacuum filtration. Cell pellets were lysed and clarified by centrifugation. Clarified supernatants were added to pre-washed mouse IgG agarose (A0919, Sigma-Aldrich) and incubated at 4°C for 1 h to sequester the immunoglobulin-binding protein Sbi. The supernatant was transferred to pre-washed M2 anti-FLAG resin (Sigma - Aldrich) and incubated at 4°C for 1.5 h. The resin was washed and incubated with 50 U of TEV protease and 100 μ g/mL FLAG peptide (Sigma-Aldrich) for 2 h at 18°C. The eluate was then collected and incubated with 0.15 U of RNase - IT (Agilent) at 20°C for 5 min. The eluate was added to pre-washed Pierce Ni - NTA magnetic agarose slurry and incubated overnight at 4°C.

The RNase III.RNA complexes were washed and the 5' ends of bound RNAs were dephosphorylated with the addition of thermosensitive alkaline phosphatase (Promega). RNA was radiolabeled by phosphorylation with T4 PNK (Sigma-Aldrich) and ³²P - γ ATP (PerkinElmer, cat no. BLU502A250UC) for 100 min at 20°C. The ³²P-radioabeled RNase III.RNA complexes were washed and unique barcoded 5' linkers and 3' App-PE adapters were ligated to the bounded RNA using 40 U T4 RNA ligase I (NEB) for each ligation step. The ³²P-radioabeled RNase III.RNA complexes were subsequently eluted in 60 μ L of 1 \times NuPAGE LDS sample buffer (Sigma-Aldrich) at 65°C for 10 min and resolved on a NuPAGE 4–12% Bis - Tris PAGE gel (Invitrogen) at 120 V for 1 h. Complexes were visualized by autoradiography using the Typhoon FLA 9500 gel imager. The band corresponding to the RNase III.RNA complex was gel-excised, fragmented, and digested with 100 μ g of proteinase K at 55°C for 2 h (Fig. S1). RNA was extracted using phenol:chloroform:isoamyl alcohol (PCI) extraction, reverse transcribed using Superscript IV (ThermoFisher), and PCR amplified. PCR products were separated on a 2% MetaPhor agarose gel (Lonza) and smeared amplicons were gel-excised using the MinElute gel extraction Kit (Qiagen). Libraries were quantified with the Qubit dsDNA HS assay kit (ThermoFisher), pooled, and submitted for HiSeq paired - end 150 bp sequencing at NovogeneAIT Genomics Singapore. RNase III-CLASH data generated in this study are available at NCBI Gene Expression Omnibus (GEO) under the SuperSeries accession number [GSE254533](https://www.ncbi.nlm.nih.gov/geo/query/acc.cgi?acc=GSE254533).

Annotation of *S. aureus* JKD6008 transcriptome

The ANNOgesic pipeline, which integrated transcriptomics data from RNA-seq, dRNA-seq, and Term-seq, was used to generate a custom annotation of the *S. aureus* JKD6009 genome in a previous report (12, 17). The features in this customized JKD6009 genome annotation were transferred to the *S. aureus* JKD6008 genome using the Rapid Annotation Transfer Tool (RATT) (31). This generated an embl output file containing the updated *S. aureus* JKD6008 genome annotation which was converted into a GFF format using EMBOSS seqret and custom scripts.

Analysis of CLASH hybrids

Analysis of the CLASH hybrids was performed similarly as described in our previous report (17). Briefly, BBDuk was used to trim the 5' adapter sequence of the raw data using the parameters "ktrim = 1 k = 23 mink = 11 hdist = 1," followed by quality trimming with the parameters "qtrim = r1 trimq = 30" (32). After trimming, BBmerge was used to merge the paired-end reads using the default parameters (33). Using the pyCRAC pipeline, demultiplexing and removal of PCR duplicates were performed using the pyBarcodeFilter.py and pyFastqDuplicateRemover.py scripts, respectively. Reads were mapped to the *S. aureus* JKD6008 genome using Novoalign (version 2.07) and read counts for each RNA species was calculated using the pyReadCounters.py script. Detection and annotation of the RNA-RNA interactions were performed using the Hyb bioinformatics pipeline and statistical analysis of these RNA-RNA interactions was calculated using custom R scripts that are outlined in a previous report (13).

Differential gene expression (RNA-seq)

Total RNA from triplicate samples of JKD6008 grown to an OD₆₀₀ of 0.8 that were either untreated or treated with 8 µg/mL vancomycin for 30 min was harvested using GTC-phenol extraction. RQ1 RNase-free DNase (Promega) was used to deplete genomic DNA and RNA was further purified using PCI extraction. Total RNA samples were sent to NovogeneAIT Genomics Singapore for paired-end 150 bp sequencing on the NovaSeq platform.

Sequencing data were pre-processed using BBtools and mapped to the *S. aureus* strain JKD6008 genome with BBmap as outlined above. Read counts for each feature were computed using bedtools coverage and differential gene expression analysis was performed using DESeq2 (34). RNA-seq data are available at NCBI GEO under the SuperSeries accession number [GSE254533](https://www.ncbi.nlm.nih.gov/geo/query/acc.cgi?acc=GSE254533).

Ribosome profiling (Ribo-seq)

The ribosome profiling protocol conducted was based on previous studies with some modifications (35–37). *S. aureus* cultures were grown to an OD₆₀₀ of 0.8 in MH media and then treated with 100 µg/mL chloramphenicol for 2 min, harvested and snap frozen in liquid nitrogen. Cell pellets were resuspended with 1 mL of cold lysis buffer (10 mM CaCl₂, 100 mM NH₄Cl, 20 mM Tris-HCl pH 8.0, 0.1% NP40, 0.4% Triton X-100, 10 U/mL RQ1 DNase [Promega], 1 mM chloramphenicol, and 100 µg/mL lysostaphin) and lysed using 3 V of zirconia beads in a FastPrep-24 5G homogenizer (MP Biomedicals) for two cycles of 40 s at 6.5 m/s with 1 min rest in between. Samples were clarified by centrifugation and 200 µL of supernatant was treated with 1,000 U of micrococcal nuclease (MNase) (Sigma-Aldrich) supplemented with a final concentration of 10 µM CaCl₂ and incubated at 25 °C shaking at 250 rpm for 1 h. Polysomes were purified using Illustra Microspin S-400 HR columns (Cytiva).

Ten micrograms of RNA were resolved on a 12% TBE-Urea polyacrylamide at 200 V for at least 4 h in 1× TBE buffer and 20–50 nt bands were gel-excised, fragmented, and recovered. The 3' ends of purified RNA were dephosphorylated with the addition of T4 PNK enzyme (New England Biolabs) and 10 mM ATP was added to phosphorylate the 5' ends of the RPF (ribosome protected fragment). RPFs were purified using PCI

extraction and unique barcoded 5' linkers were ligated to the purified RPF. The 5' end ligated samples were purified using PCI extraction and then the 3' App-PE adapters were ligated to the RPF using 40 U T4 RNA ligase I (NEB). The 5' and 3' ligated samples were resolved on a 12% TBE-Urea polyacrylamide gel and the band corresponding to the RPF was gel-excised, fragmented, and recovered. Purified RPFs were reverse transcribed using Superscript III (ThermoFisher) and rRNA depletion was performed using the Zymo-Seq RiboFree Total RNA Library Kit (Zymo Research) with two modifications: the first-strand cDNA synthesis and adapter ligation steps were omitted. The cDNA was rRNA depleted at 68°C for 14 h, PCR amplified, separated on a 2% MetaPhor agarose gel (Lonza) and then gel-excised using the MinElute gel extraction kit (Qiagen). Libraries were quantified with the Qubit dsDNA HS assay kit (ThermoFisher), pooled and submitted for HiSeq paired - end 150 bp sequencing at NovogeneAIT Genomics Singapore.

Sequencing data were pre-processed using BBtools and mapped to the *S. aureus* strain JKD6008 genome with BBmap as outlined above. Read counts for each feature were computed using bedtools coverage. Ribo-seq data are available at NCBI GEO under the SuperSeries accession number [GSE254533](https://www.ncbi.nlm.nih.gov/geo/query/acc.cgi?acc=GSE254533).

Protein extraction and mass spectrometry (LC-MS/MS)

S. aureus cultures were grown to an OD₆₀₀ of 0.8 in MH media and treated with 8 µg/mL vancomycin for 30 min. Cultures were harvested by centrifugation and cells pellets were resuspended in 1 mL of lysis buffer (50 mM Tris-HCl [pH 7.8] [Sigma-Aldrich], 150 mM NaCl, and 1 tablet "cOmplete" EDTA - free protease inhibitor [Roche] per 50 mL). The cell resuspension was lysed with 3 V of zirconia beads in a FastPrep-24 5G homogenizer (MP Biomedicals) for two cycles of 40 s at 6.5 m/s with 1 min rest in between. Cell lysates were cleared by centrifugation and protein concentration was quantified using the Qubit Protein and Protein Broad Range Assay Kit (ThermoFisher). Protein samples were sent to the UNSW Bioanalytical Mass Spectrometry Facility for liquid chromatography-mass spectrometry (LC-MS/MS) processing and analysis using the Orbitrap Fusion Lumos Tribrid Mass Spectrometer (ThermoFisher).

Raw mass spectrometry data were processed using the MaxQuant program (38). The Mascot search engine was used to match peptides in the raw mass spectrometry data against the whole *S. aureus* reference proteome set in the UniProt database (39). Using Perseus, contaminants were filtered and label-free quantification (LFQ) values were log₂ transformed. Peptides that did not contain LFQ-intensity values in at least 70% of total samples were removed and missing values were imputed using width and downshift values of 0.3 and 1.8, respectively. The difference in log₂(LFQ) values between the control and vancomycin-treated group was then calculated (40). The statistical significance of these log₂(LFQ) differences was calculated using a two-tailed student *t* test and then FDR corrected using the Permutation-based FDR method. The mass spectrometry proteomics data have been deposited to the ProteomeXchange Consortium via the PRIDE partner repository (<https://www.ebi.ac.uk/pride/>) with the data set identifier [PXD049022](https://www.ebi.ac.uk/pride/entry/PXD049022).

Data clustering (SOMs)

Data normalization and compilation of multi-omics data table

The untreated samples were analyzed using RNA-Seq, Ribo-Seq, and LFQ proteomics. The transcriptomics and proteomics data sets both had three biological replicate samples each for the untreated controls, while the Ribo-seq experiment had biological duplicate samples. Each biological replicate sample was log₂ normalized, and the average value from the biological replicate samples and from each type of -omics data set were calculated independently. The resulting averaged values were further normalized using the z-normalization to calculate the standard score. The standard score represents the number of sample standard deviations by which the average log-transformed abundance value of a single transcript or protein is above or below the mean value for the sample. A kernel density plot and normal Q-Q plot were generated

to ensure that the data appear normally distributed after z-score normalisation. The standard scores were combined into a single multi-omics data table, with transcript, ribosome occupancy, and the corresponding protein product as rows and the samples from different types of -omics and treatments as columns.

Enrichment of binding targets of sRNA from co-regulated clusters of transcripts and protein products

SOMs were used to identify co-regulated clusters of transcripts and protein products from the multi-omics data. Here, the SOMs function from the R package Kohonen v3.0.11 (41) was used to divide *S. aureus* genes into three clusters based on their gene expression profile across all untreated samples using the single multi-omics data table and JKD6008 genome annotation GFF file as inputs. The co-regulated transcript and/or protein products from each cluster were analyzed for enrichment of verified sRNA-mRNA interactions in *S. aureus* and RNase-III CLASH interactions using Fisher's exact test. For each cluster that contained RNase III-CLASH interactions, a metagene plot of the cumulative count of RNA-RNA interactions relative to the start codon was generated using a custom script.

Construction of GFP-translational fusions

Three target mRNAs *lip*, *SAA6008_01130*, and *hpr* were PCR amplified from the JKD6008 gDNA using Phusion Hot Start Flex Polymerase (New England Biolabs) with primers that incorporate the BglIII and EcoRV restriction sites at the 5' and 3' ends, respectively. PCR amplicons were cloned into pCN33p::ptufA-isaA-GFP by switching out the *isaA* insert between the BglIII/EcoRV sites. Small RNAs of interest (RsaOI, RNAIII, and RsaE) were amplified with primers that incorporate the PstI and EcoRI restriction sites at the 5' and 3' ends, respectively. Purified amplicons were cloned into a pICS3::P_{tufa} vector (42) and after verifying the constructs by Sanger sequencing, the pICS3::P_{tufa} construct was transformed into electrocompetent *S. aureus* RN4220 and overnight cultures were stored at -80°C with 16% (vol/vol) glycerol. To generate co-transformants, the transformed strains were then made electrocompetent and subsequently transformed with the pCN33 vector.

Flow cytometry measurement of GFP expression

S. aureus RN4220 strains co-transformed with the target GFP-translational fusion and sRNA expression plasmid were streaked onto BHI agar supplemented with 10 µg/mL chloramphenicol and erythromycin. For each sample, three biological replicates were individually inoculated into 1 mL of 0.22 µM filtered BHI media and incubated overnight at 37°C with 200 rpm shaking. Cultures were subsequently normalized to an OD₅₇₈ of 2 using 0.22 µM filtered BHI media and fluorescence was quantified with the LSRTorressa Special Order Research Product cell analyser (BD Biosciences) using a 530/30 nm bandpass filter. The forward scatter, side scatter, and background cellular fluorescence were gated initially on a wild-type RN4220 population and at least 100,000 events were sampled. The median fluorescence intensity (MFI) for each biological replicate was determined using the FlowJo software (version 8) and a standard two-tailed student's *t* test was performed to determine the difference in mean MFI between samples.

Antibiotic sensitivity testing by spot dilution

S. aureus strains JKD6009, JKD6008, and Mu50 containing the pSD1 constructs were inoculated into 5 mL of MH media supplemented with 10 µg/mL chloramphenicol and incubated overnight at 37°C with 200 rpm shaking. Cultures were then normalized to an OD₆₀₀ of 1, aliquoted into a 96-well microtiter plate (Corning), serially diluted (up to 10⁻⁷) in MH media and spotted onto solid MH plates supplemented with 500 ng/mL aTC, 5 µg/mL chloramphenicol, and with 0, 1, 2, or 3 µg/mL vancomycin. Spot plates

were air-dried at room temperature and then incubated at 37°C for 24–48 h. Results were imaged on the Bio-Rad Chemi-doc using the default trans-white light settings.

Antibiotic sensitivity testing by growth curve analysis

Growth curve analysis of *S. aureus* strains JKD6008, JKD6009 and other strain derivatives in the presence of different antibiotics were measured using the Bioscreen C MBR (Growth Curves USA, Piscataway, NJ). Here, single colonies were inoculated into 5 mL of MH media and incubated at 37°C shaking at 200 rpm overnight. Overnight cultures were normalized to an OD₆₀₀ of 2 and biological triplicates were diluted 1/100 into three wells containing 200 µL of MH media supplemented with either 0, 2, 3, or 4 µg/mL of vancomycin. Three wells containing only MH media were used as blanks. The plate was incubated in the Bioscreen C at 37°C with continuous low shaking and OD₆₀₀ readings were recorded every 20 min for 24 h. Growth curve data were analyzed using GraphPad Prism.

Northern blot analysis

Total RNA purified (2 µg) from GTC-phenol:chloroform extraction was resolved on a 12% TBE-Urea polyacrylamide gel and electrophoresed at 200 V for at least 4 h in 1× TBE buffer. The gel was post-stained with SYBR Safe DNA Gel Stain and intact RNA was confirmed using the Bio-Rad Chemi-doc. The RNA was transferred onto a nylon membrane (GE Healthcare Life Sciences) soaked in 0.5× TBE buffer via electrophoresis at 30 V for 4 h at 4°C and then crosslinked in a Strategene Auto-crosslinker with 1200 mJ UV-C. The membrane was pre-hybridized in ULTRAhyb-Oligo buffer (ThermoFisher) at 37°C for 30 min. The 35 mer DNA oligonucleotide probes were radiolabeled with ³²P-ATP at 37°C for 1 h and then purified over a G50 size exclusion column (GE Healthcare Life Sciences) following the manufacturer's instructions. The purified oligonucleotide mix was added to the nylon membrane and hybridized at 37°C overnight. The membrane was washed four times in wash buffer (2× subsp. buffer [Sigma-Aldrich] and 0.1% SDS) at 37°C for 30 min. Afterward, the membrane was exposed on a BAS Storage Phosphor Screen and detection of the hybridized probe was performed on the LAS-3000 (Fujifilm).

RESULTS

RNase III-CLASH uncovers the VISA sRNA interactome

In our earlier analysis, we used RNase III-CLASH to profile RNA-RNA interactions associated with RNase III in the methicillin-resistant *S. aureus* isolate JKD6009 (12, 17). In an effort to capture sRNA interactions that contribute to vancomycin tolerance we have applied RNase III-CLASH to the clinical VISA strain JKD6008. To facilitate the purification of UV-crosslinked RNA-protein complexes from VISA, we first constructed a chromosomal translational fusion of RNase III with a C-terminal linked His₆-TEV-FLAG dual affinity tag in *S. aureus* VISA strain JKD6008. JKD6008 has a thicker cell wall compared to the JKD6009 parent strain (2), and our initial RNase III purifications were unsuccessful. We found that the inclusion of 10 µg/mL lysostaphin and lysis for two cycles of 40 s using a Fast-Prep-24TM 5G homogenizer (MP Biomedicals) increased cell lysis and recovery of RNase III in the soluble fraction, but the harsher lysis conditions also resulted in the release of an approximately 50 kDa protein that bound to the M2 FLAG resin. LC-MS/MS analysis indicated that the FLAG-purified protein was the immunoglobulin-binding protein, Sbi. To remove Sbi and improve RNase III recovery, we incubated our cell lysates with mouse IgG agarose to sequester Sbi. After removing Sbi from the cell lysate, we were able to purify RNase III-HTF complexes from VISA cell lysates.

Biological duplicates of RNase III-CLASH libraries were prepared from *S. aureus* JKD6008 and the isogenic His-TEV-FLAG tagged strain *mnc*-HTF as described previously (excepting improved lysis conditions described above) (17). Briefly, cultures grown to an OD₆₀₀ of 0.8 were treated with and without 8 µg/mL vancomycin for 10 min. Cultures were then immediately crosslinked with 400 mJ of UV-C (Vari-X-Link, UV03), harvested by

vacuum filtration, and lysed as described above. RNase III-associated RNAs were affinity purified under denaturing conditions and linkers ligated to RNA-protein complexes followed by cDNA library construction.

RNase III-associated RNAs were sequenced and analyzed using the snakemake pipeline Hyb-CRAC-R that incorporates the pyCRAC package (43) for identifying protein binding sites, *hyb* (44) that identifies RNA-RNA interactions, and our statistical analysis of RNA hybrids in the CLASH data set. From these analyses, 775 statistically significant RNA-RNA interactions were recovered from VISA strain JKD6008 including 170 sRNA-RNA interactions (Fig. 1). To assign RNA fragments recovered by CLASH to genomic features, the genome annotation previously generated for the parental MRSA strain JKD6009 was transferred to the isogenic VISA isolate JKD6008 using RATT (31). This annotation incorporated RNA boundaries determined by dRNA-seq and Term-seq, and includes experimentally determined mRNA 5' and 3' UTRs. The 755 RNA-RNA interactions in VISA covered a broad range of RNA classes (Fig. 2A) and consistent with earlier work, mRNA-mRNA interactions are the most recovered interaction type supporting the idea that *S. aureus* may utilize regulatory mRNA interactions to control gene expression (17). A metagene analysis showed that both RNA-RNA and sRNA-RNA interactions were enriched at the start codon, which corresponds to the canonical mechanism of sRNA regulation by occluding the RBS (Fig. 2B). Comparison of the VISA and

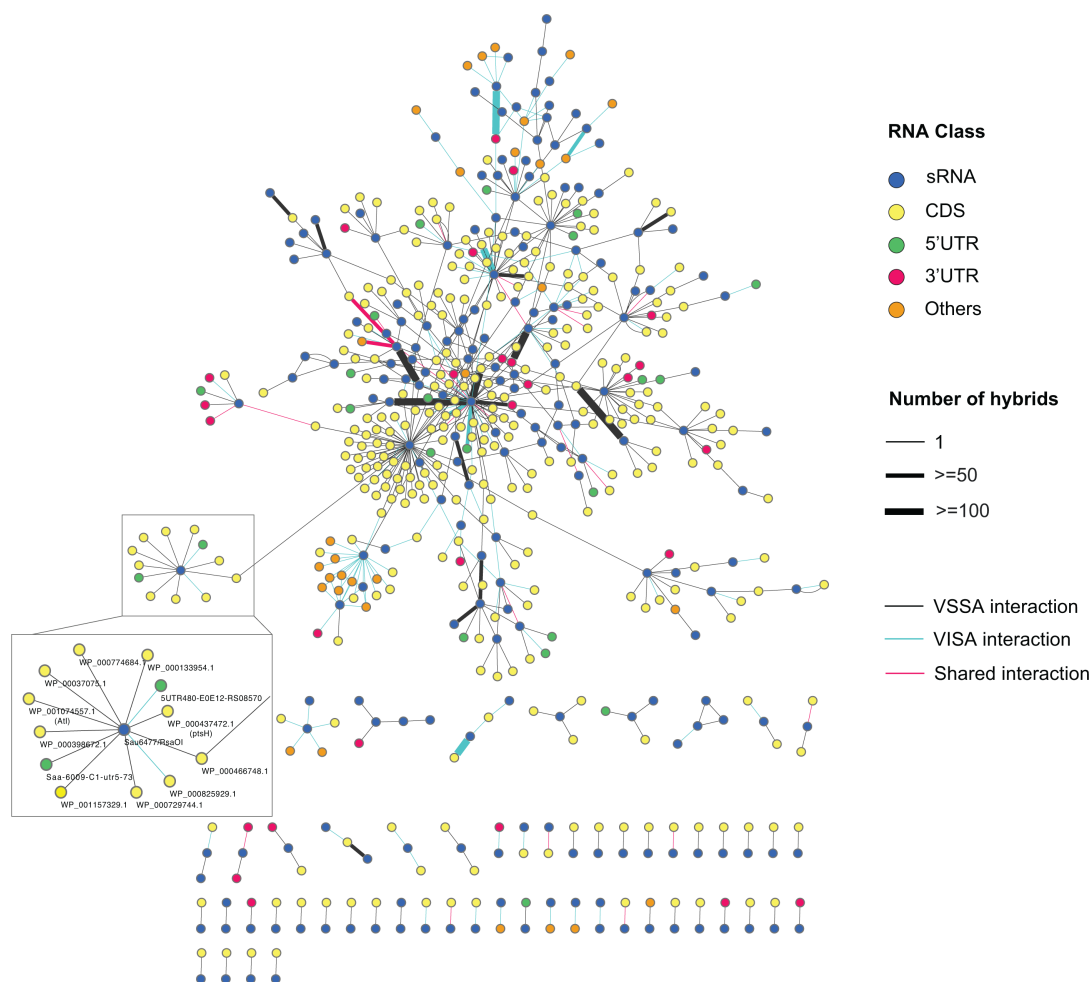


FIG 1 Small RNA interactome of *S. aureus* strains JKD6008 (VISA) and JKD6009 (VSSA). Each RNA is represented as a node (circles) and are colored according to its RNA class as indicated by the legend (top right). RNA-RNA interactions (FDR < 0.05) are represented as edges (lines) and the thickness of each edge represents the hybrid count for each RNA-RNA interaction. Individual RNA-RNA interactions captured in JKD6008 and JKD6009 are represented as blue and black edges, respectively (bottom right).

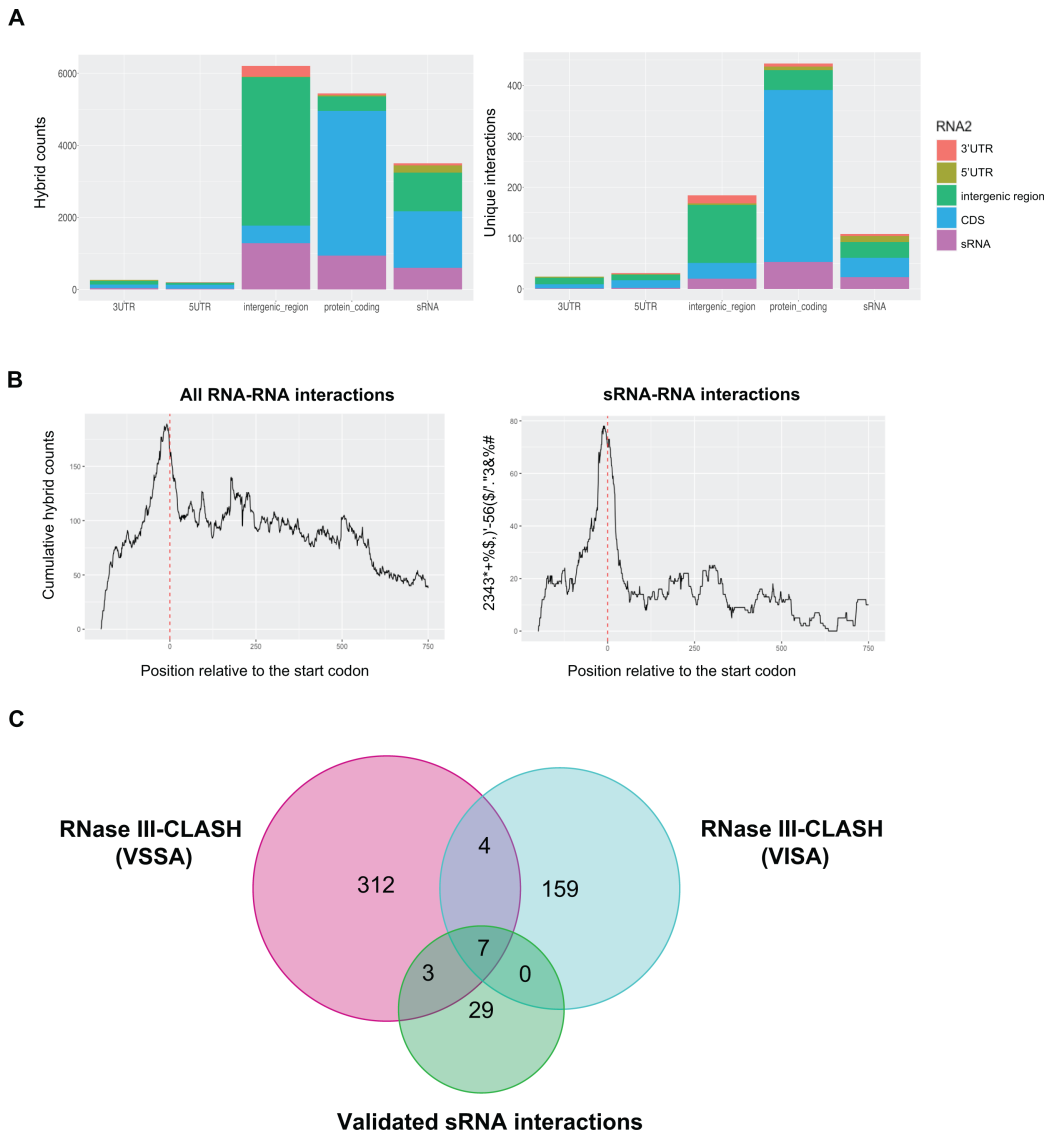


FIG 2 RNA-RNA interactions recovered by RNase III-CLASH in vancomycin-tolerant *S. aureus* strain JKD6008 (VISA). (A) Histogram of RNA classes recovered by JKD6008 RNase III-CLASH. The total number of hybrid reads (PCR duplicates collapsed, left panel) and the number of unique RNA-RNA interactions (right panel). RNA classes for hybrid read halves are indicated (right). Note that multiple hybrid reads can represent a single (unique) RNA-RNA interaction. (B) Metagenetic plot of the cumulative count of RNA-RNA (left) and sRNA-RNA (right) interactions relative to the mRNA start codon as indicated by the red dashed line. (C) Venn diagram of interactions shared between the sRNA interactomes of VISA (JKD6008), VSSA (JKD6009), and experimentally validated *S. aureus* sRNA-mRNA interactions from the literature.

vancomycin-sensitive *S. aureus* (VSSA) sRNA-RNA interactomes, which includes JKD6009 and USA300, revealed that 11 sRNA-RNA interactions are shared between the MRSA and VISA interaction networks, 7 of which were have been experimentally validated including RsaA-RNAIII, RNAIII-*esxA*, RsaOG-RsaE, SprX2-*spoVG*, RsaA-*mgrA*, and RsaA-*ssaA* (12, 45, 46)(Fig. 2C). The small amount of overlap between these data sets likely reflects the small size of the VISA data set and sampling of a large sRNA interactome rather than a large divergence in the VISA and VSSA interaction networks.

To determine the potential biological functions of sRNAs, the VISA and MRSA sRNA interactomes were merged and each sRNA node was extracted for GO term analysis of the associated mRNAs. GO term analysis revealed that 26 sRNA clusters were enriched for

GO terms associated with several biological processes including purine ribonucleotide synthesis, methylation, and hexose metabolism ($P < 0.05$) (Table S3).

Clustering reveals post-transcriptionally regulated mRNAs with RNase III-CLASH sRNA-mRNA interactions

Our RNase III-CLASH data provide a snapshot of the VISA sRNA interactome but does not inform on the function of the sRNA-mRNA interaction (e.g., activation, repression, transcript degradation, and translational repression). Further, a proportion of experimentally verified sRNA-mRNA interactions recovered by proximity-dependant ligation are reported to not affect the expression of the target mRNA (14, 19).

We aimed to identify sRNA-mRNA interactions that activate or repress mRNA translation by using a multi-omics approach. Previous work indicates a strong correlation between mRNA and protein abundance within the cell. Many genes that deviate from this correlation are known targets of post-transcriptional regulators (47). To identify genes that are being post-transcriptionally regulated, we collected RNA-seq, Ribo-seq, and proteomics data for *S. aureus* strain JKD6008 (VISA) during mid-exponential growth in Muller-Hinton media. For each biological replicate sample from the RNA-seq, Ribo-seq, and proteomics data sets, the average expression value for each condition was calculated across biological replicates in each omics datatype. We found a high level of correlation between our RNA-seq and Ribo-seq data sets (Pearsons correlation 0.8 from 2,679 genes) and a lower correlation between RNA-seq and proteomics data (Persons correlation 0.32 from 566 genes) (Fig. S2).

To convert the distributions of values to the same scale, the average expression values for each -omics data set were transformed to z-scores and the data sets were confirmed to be normally distributed (Fig. S3). SOMs were used to cluster genes with similar z-score normalized transcriptional and translational values (27, 48). We used 39 experimentally verified *S. aureus* sRNA-mRNA interactions from past literature (Table S4) to determine if we could enrich functional sRNA-mRNA interactions using SOMs clustering (Fig. 3). Three clusters of genes with different transcriptional and translational patterns were generated using SOMs. Cluster 1 is enriched for verified translationally repressive sRNA-mRNA interactions (9/35 within cluster 1, Fisher's exact test, $P = 0.0198$) (Fig. S4A). The 173 genes in cluster one exhibit a pattern of average to high transcript and RPF abundance, but lower protein levels, suggesting that the genes in this cluster are being post-transcriptionally repressed (Fig. 3). The 187 genes in cluster 2 have transcript abundance that corresponds with protein expression, while the 207 genes in cluster 3 appear to collectively have moderately higher protein levels relative to transcript and RPF abundance, which suggests either enhanced transcript stability and/or translational activation (Fig. 3).

Next, we cross-referenced the 412 *S. aureus* sRNA-mRNA interactions captured from both the VISA and VSSA sRNA interactome with the three SOMs clusters (Fig. 3; Fig. S4B). Both clusters 1 and 2 are enriched for sRNA-mRNA interactions captured in our RNase-III CLASH network (Fisher's exact test, $P < 0.0001$) and we predicted that these clusters may be used to identify functionally repressive sRNA-mRNA interactions.

As cluster 1 has lower than expected protein abundance and verified repressive sRNA-mRNA interactions, we speculated that this cluster is enriched for translationally repressive RNase III-CLASH interactions. We examined whether cluster 1 interactions are enriched around the 5' UTR and start codon since sRNAs canonically interact with this region to repress translation. Metagene plots of the subset of RNase-III CLASH sRNA-mRNA interactions detected in each cluster were used to determine which regions of the mRNA were being targeted for sRNA regulation. For the 88 sRNA-mRNA interactions in cluster 1, the mRNA read halves predominantly mapped to the 5' UTR and start codon and there is also some enrichment of mRNA reads along two segments of the coding regions (Fig. S4Ci). A slightly less pronounced enrichment was recovered for clusters 2 and 3 across the 5' UTR and start codon region as well as 250–500 nt downstream of the start codon. We note that many CDS starts are <500 nt apart suggesting that the

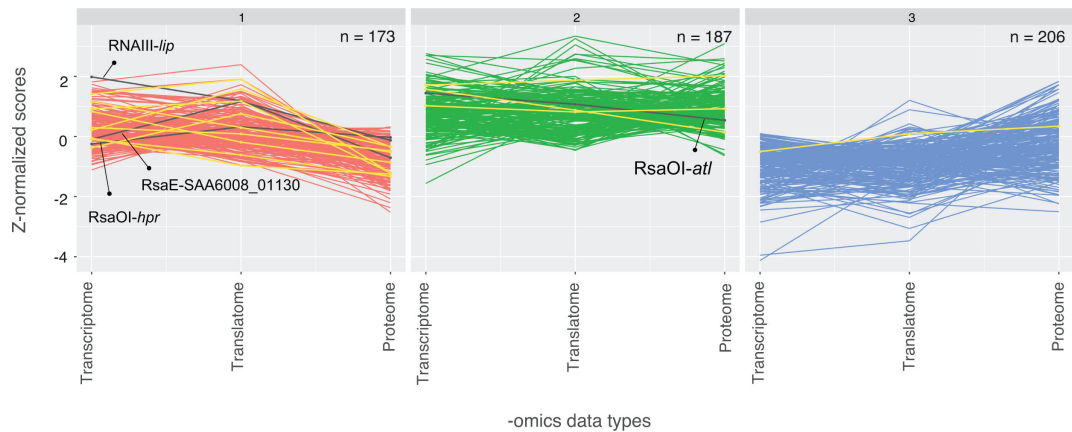


FIG 3 Self-organizing maps (SOMs) reveal a cluster of genes enriched with translationally repressive sRNA-mRNA interactions. Each graph displays a SOMs cluster of genes with similar transcriptional and translational patterns. The x-axis contains the -omics data types for RNA-seq (transcriptome), Ribo-seq (translatome), and mass spectrometry (proteome) under the control conditions. The y-axis contains the z-normalized scores for all the -omics data types. The number of genes present in each cluster (from a total of 566 genes with signal in all data sets) is indicated (N) in the top right of each plot. Verified *S. aureus* sRNA-mRNA interactions are indicated in yellow and four RNase III-CLASH interactions tested in this study are indicated in black.

downstream peak is likely associated with a downstream CDS start rather than a specific internal site within coding sequences (Fig. S4Cii&iii).

Previous work indicated that functional sRNA-mRNA interactions are more likely to contain a higher number of hybrid reads (19). We examined the number of hybrid reads recovered for sRNA-mRNA interactions in each cluster (Fig.S5). While cluster 1 contains many of the highest abundance interactions, no statistically significant difference was observed between the three clusters.

Collectively our data indicate that clustering of genes with lower than expected protein abundances enriches for experimentally verified and CLASH-recovered sRNA-mRNA interactions.

SOMs cluster 1 contains sRNA-mediated translationally repressed genes

Our SOMs analysis suggests that sRNA interactions with mRNAs in cluster 1 may be responsible for translational repression of the gene (lower than expected protein abundance). To evaluate their function, three sRNA-mRNA interactions from our RNase-III CLASH network that were present in cluster 1 were tested using GFP-translational fusions: RNAIII-*lip*, RsaE-SAA6008_01130, and RsaOI-*hpr*. Each target mRNA was cloned into the GFP-translational fusion vector pCN33::P_{tufA}. Each mRNA was cloned from the +1 transcriptional start site identified by dRNA-seq and included the native Shine-Dalgarno sequence that overlaps the predicted CLASH interaction site. These were transformed into *S. aureus* RN4220 strains containing the pICS3::P_{tufA} vector constitutively expressing their cognate regulatory sRNA and fluorescence was measured using a flow cytometer. Transcription of the sRNAs RNAIII and RsaE reduced the fluorescence signal of the triacylglycerol lipase precursor *lip* and SAA6008_01130, which encodes an acetyltransferase family protein, by 2.05- and 3.10-fold (both $P < 0.05$), respectively (Fig. 4A and B). RsaOI reduced *hpr* expression by 5.16-fold ($P < 0.05$) (Fig. 4C). All three sRNA-mRNA interactions significantly reduced target mRNA translation.

Collectively our data suggest that translationally repressive sRNA-mRNA interactions are enriched in clusters with a lower than expected protein abundance. The correlation in transcript and protein abundance may provide a useful tool to identify post-transcriptionally regulated genes and functional sRNA-mRNA interactions.

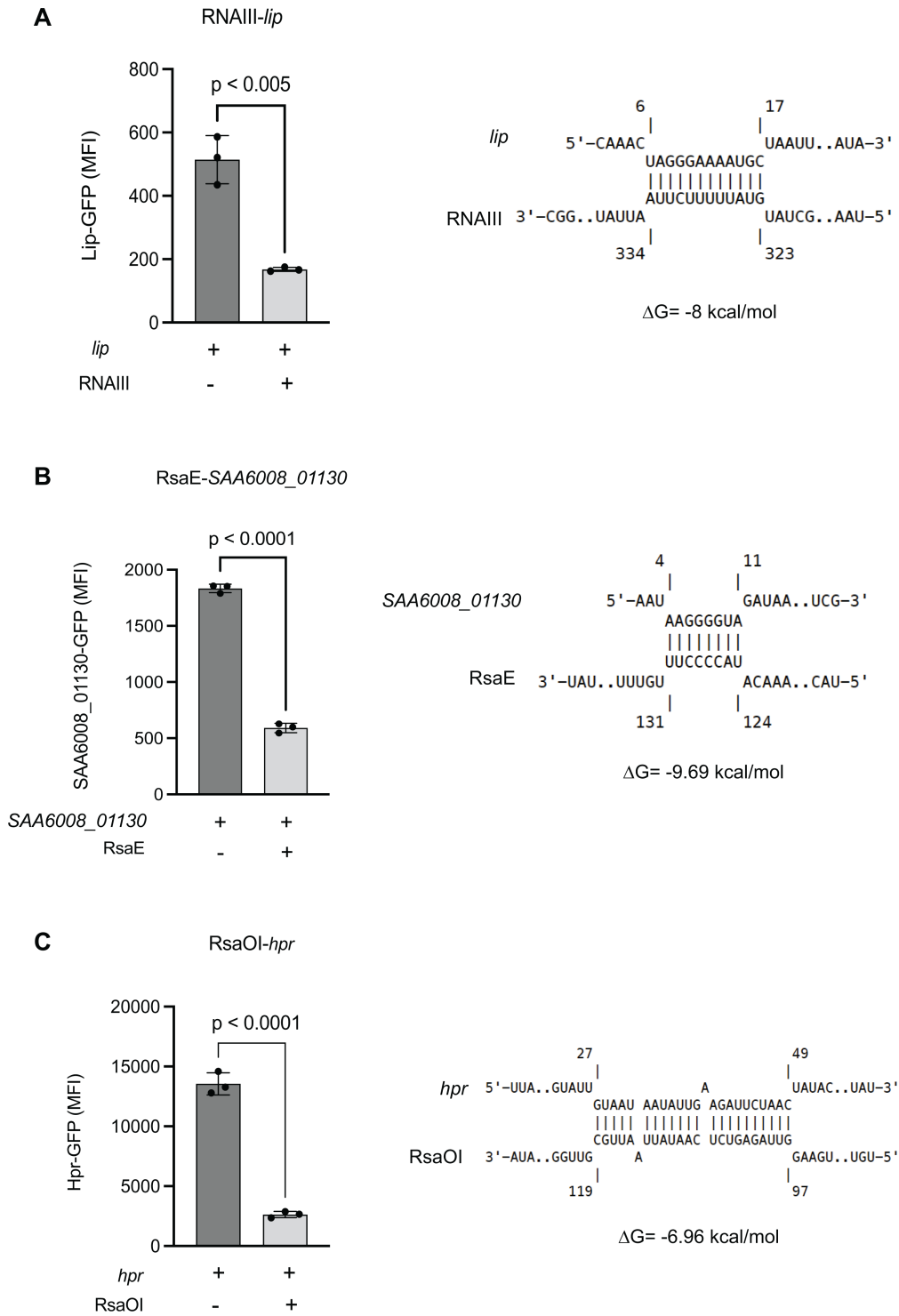


FIG 4 Translationally repressive RNase III-CLASH sRNA-mRNA interactions in SOMs cluster 1. GFP-translational fusions for *lip* (A), SAA6008_01130 (B), and *hpr* (C) were constitutively expressed in *S. aureus* strain RN4220 with or without transcription of their cognate sRNAs (indicated above). IntaRNA predicted interactions at mRNA site recovered by RNase III-CLASH and the associated free energy change are indicated on the right. Median fluorescence intensity was measured using flow cytometry and error bars indicate standard error. *P* values were calculated using a two-tailed *t* test.

The small RNA RsaOI is induced by vancomycin

We next looked to use our VISA CLASH network and meta-omics clustering to identify sRNAs and interactions that contribute to vancomycin tolerance. We performed RNA-seq on VISA samples that were treated with 8 $\mu\text{g}/\text{mL}$ vancomycin for 30 min (Fig. 5A). RsaOI was the highest upregulated sRNA in response to vancomycin treatment ($\log_2\text{FC} = 5.91$, aka Teg47 or Sau6477). Differential RNA sequencing (dRNA-seq) and Term-seq data were used previously to map the transcriptional start sites and termination sites in *S. aureus* JKD6009 genome (17) and indicate that RsaOI is 292 nt long transcript (Fig. 5B), which is slightly larger than earlier northern analysis (49). Northern blot analysis demonstrated a dose-dependent induction of RsaOI in response to vancomycin treatment (Fig. 5C). The vancomycin-responsive WalkR two-component system is an important contributor to the VISA phenotype. To determine whether RsaOI expression is under the control of WalkR, northern blot analysis for RsaOI was performed in wild-type USA300 strain NRS384, ΔyycH1 , and $\text{walk}^{\text{H271Y}}$ mutants with and without 8 $\mu\text{g}/\text{mL}$ vancomycin. RsaOI was induced similarly to wild type in the walkR mutants, indicating that it is not regulated by WalkR (Fig. S6). To test vancomycin tolerance, JKD6008 and ΔrsaOI were grown in MH media in the presence or absence of sub-MIC vancomycin (3 $\mu\text{g}/\text{mL}$). These results indicate that rsaOI is strongly induced by vancomycin but is not required for vancomycin tolerance (Fig. S7).

RsaOI controls the expression of the major autolysis *Atl* critical to vancomycin tolerance

To identify functional targets of RsaOI, we looked within our CLASH data using the SOMS clustered mRNA targets. RsaOI has nine differentially expressed RNase III-CLASH mRNA targets (Fig. 6A) and five of these are downregulated during treatment with vancomycin using a $\log_2\text{FC}$ cutoff $\geq |0.5|$ (Fig. 6B), suggesting that the RsaOI upregulation causes the repression of these mRNA targets. To identify functional RsaOI targets, we repeated our SOMS clustering on RNA-seq and proteomics data and included vancomycin-treated VISA cultures (Fig. 6C). In our earlier analysis, we found a strong correlation between our RNA-seq data and Ribo-seq data. As the Ribo-seq data did not add significantly to our ability to cluster genes, we omitted these data from our analysis. We segregated the data into three clusters that separated the omics data into distinct profiles. Cluster 3 is enriched for experimentally verified sRNA targets and has lower protein abundance than expected from mRNA levels. One RsaOI mRNA target (RsaOI-hpr) falls within cluster 3 when we overlay our RNase III-CLASH network, and we had previously confirmed that this interaction is functional (above). Interestingly, three targets fall within cluster 1 which shows correlated RNA and protein levels. Within this cluster, SAA6008_01438 displays higher protein abundance compared to transcript levels. We focused on the mRNA *atl* in cluster 1 that encodes a bifunctional autolysin involved in cell wall turnover and cell division as this has previously been implicated in glycopeptide tolerance (50, 51). RNase III-CLASH predicted that RsaOI binds to the coding region of *atl* mRNA consistent with mRNA decay rather than translational repression as the mechanism of action (Fig. 6C). After treatment with vancomycin, *atl* mRNA and protein are downregulated to a similar extent consistent with the profile of cluster 1 (Fig. 6B and D). We used a GFP-translational fusion to evaluate the function of RsaOI on *atl* gene expression (Fig. 6E). The transcription of RsaOI reduced the fluorescence signal of *Atl*-GFP by 1.52-fold ($*P < 0.05$). Point mutations introduced into the predicted seed regions of either RsaOI or *atl* increased expression modestly ($P \leq 0.05$), and full repression was restored when both compensatory mutations were simultaneously expressed together ($P \leq 0.01$) confirming a direct interaction (Fig. 6E and F). The RNase III-CLASH interaction indicates that RsaOI base pairs 226 nt downstream of the start codon of *atl* mRNA (Fig. 6F). We speculate that RsaOI recruits RNase III to the coding sequence of *atl* mRNA and drives repression through mRNA degradation resulting in more correlated mRNA and protein abundance. We used RT-qPCR to measure *atl* mRNA abundance in the ΔrsaOI strains. Deletion of *rsaOI*

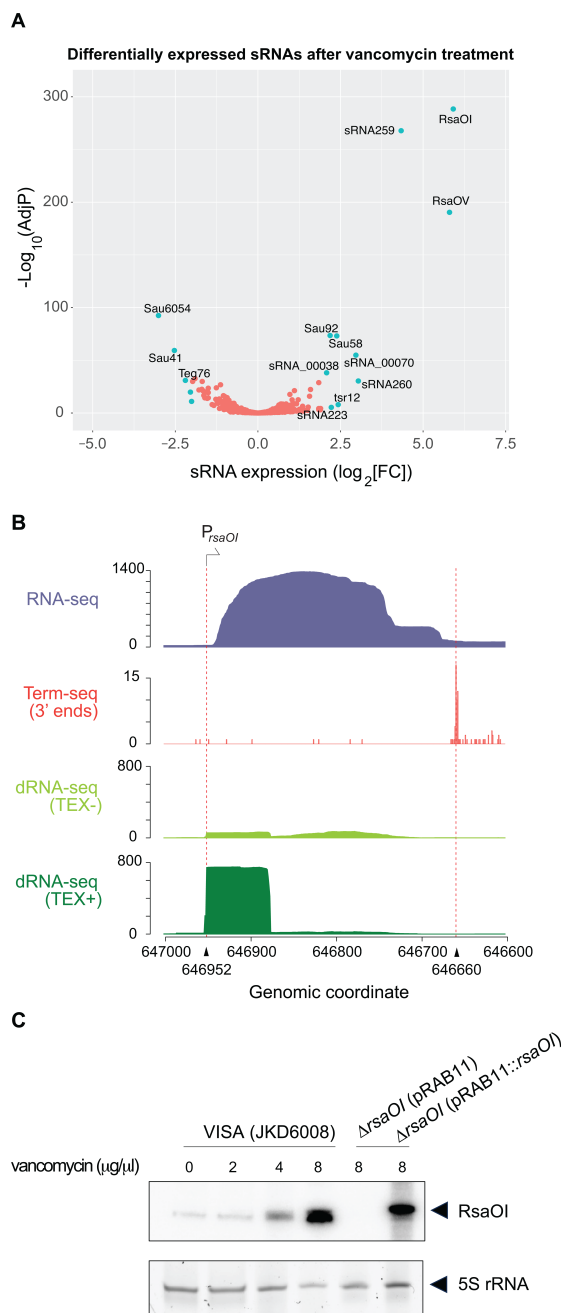


FIG 5 RsaOI is induced by vancomycin stress. (A) Volcano plot of differentially expressed sRNAs in JKD6008 after 30 min of treatment with 8 μ g/ μ L vancomycin treatment. Small RNAs with $\log_2FC \geq |2|$ and FDR < 0.05 are indicated in light blue. (B) 5' and 3' end mapping of RsaOI. From top to bottom, total RNA-seq reads (blue), Term-seq RNA 3' end reads after vancomycin treatment (red), dRNA-seq reads after vancomycin treatment (no TEX treatment), dRNA-seq reads after vancomycin treatment (with TEX treatment). Dashed red lines indicated RsaOI 5' and 3' ends determined by dRNA-seq and Term-seq. (C) Northern blot analysis of RsaOI expression after 30 min of treatment with increasing vancomycin concentrations (indicated above) in VISA (JKD6008) and the isogenic Δ *rsaOI* mutant. Migration of RsaOI is indicated by the black arrow. Sybr-stained 5S rRNA is included as a loading control.

increases *atl* abundance 2.59-fold consistent with RsaOI directing cleavage of the transcript.

Atl is downregulated in VISA strains compared to the VSSA parent strains and we assessed vancomycin tolerance of an *atl* knockdown. The *atl* CRISPRi knockdown

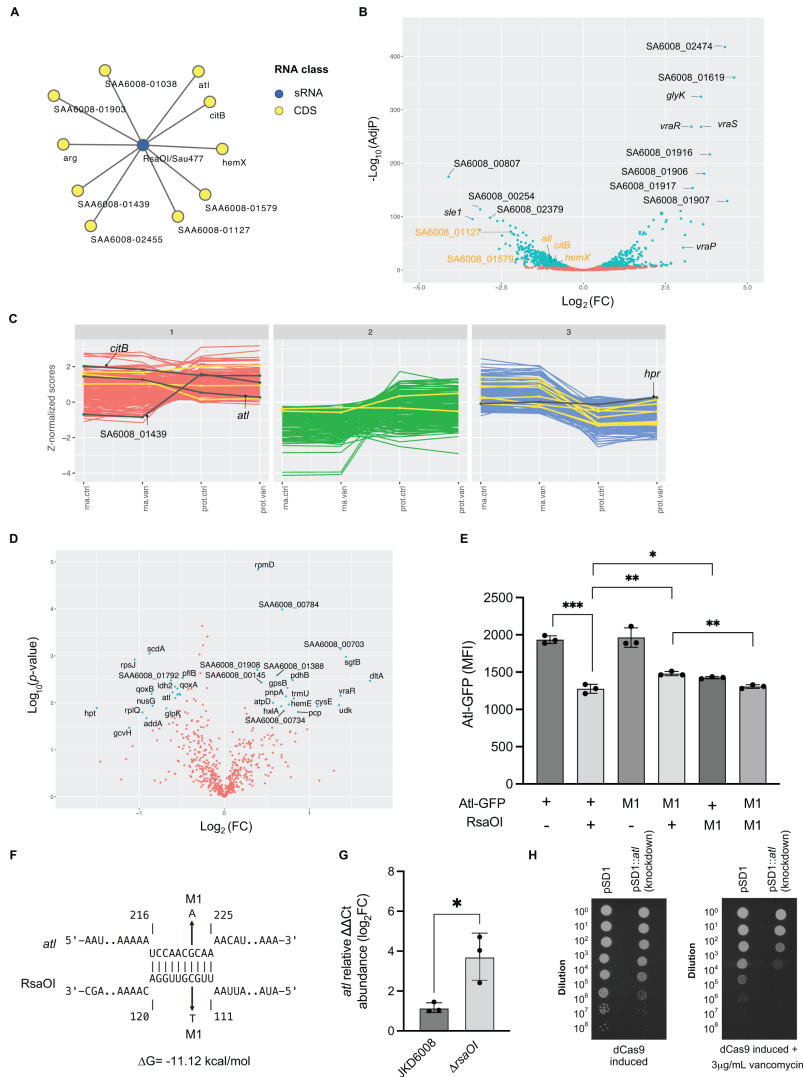


FIG 6 RsaOI mediates the expression of the autolysin AtI. (A) The sub-network of RNase III CLASH RNA-RNA interactions with RsaOI (blue node). Yellow nodes indicate mRNA targets (indicated). (B) Volcano plot of differentially expressed mRNAs in vancomycin treatment (8 μ g/mL for 30 min) VISA strain JKD6008. RNase-III CLASH identified mRNA targets of RsaOI are highlighted with orange text. Differentially expressed genes that are statistically significant $\log_2FC \geq |2|$ and $FDR < 0.05$ are indicated in light blue. (C) SOMs clustering of genes with similar transcriptional and translational expression patterns. The x-axis contains the -omics data types for RNA-seq (transcriptome, “rna”) and mass spectrometry (proteome, “prot”) under control conditions (.ctrl) or with vancomycin treatment (.van). The y-axis contains the z-normalized scores for all the -omics data types. Experimentally validated *S. aureus* sRNA-mRNA interactions are indicated in yellow. RNase III-CLASH identified RsaOI mRNA targets are indicated in black with labels. (D) Proteomic analysis of VISA strain JKD6008 with and without vancomycin treatment. Statistical significance was determined using the permutation-based FDR corrected *t* test and differentially expressed proteins with an $FDR < 0.05$ are indicated in light blue. (E) The GFP-translational fusion for the *atl* gene was constitutively expressed in *S. aureus* strain RN4220 with or without transcription of RsaOI (indicated below). RNase III-CLASH predicted an interaction within the coding region of *atl* which is indicated on the right. Median fluorescence intensity was measured using flow cytometry and error bars indicate standard error. *P* values were calculated using a *t* test (indicated above plot). (F) Spot plate dilution assays to assess vancomycin tolerance in CRISPRi knockdown of *atl* in VISA strain JKD6008. Vector control (pSD1) and CRISPRi *atl* knockdown (pSD1-*atl*) are indicated on the top of the plate and the serial 10-fold dilutions from 10^0 to 10^{-7} are labeled on the left. Lane 1: JKD6008 pSD1 vector control. Lane 2: JKD6008 pSD1-*atl* (CRISPRi knockdown).

displayed an approximately 10-fold reduction in growth under the control condition relative to the vector control. In the presence of sub-MIC vancomycin (3 $\mu\text{g}/\text{mL}$), the reduction in growth for the *atl* CRISPRi knockdown increased 100-fold (Fig. 6F). This suggests that *Atl* is required for normal growth and this growth defect is exacerbated in the presence of vancomycin. Increased *Atl* levels in the *rsaO1* deletion strain may contribute to increased growth under vancomycin stress.

DISCUSSION

A wealth of sRNA interactome data has been collected in recent years using proximity-dependant ligation techniques including CLASH, RIL-seq, iRIL-seq, and HiGRIL-seq (13–16, 18, 52). While these data sets provide evidence of sRNA-mRNA interactions, they do not indicate the function of the interactions (e.g., activating, repressing, target decay, and translational control). In addition, it appears that these data sets contain a subset of abundant sRNA-mRNA interactions that do not control target mRNA expression. Discriminating between the different functional sRNA interactions and those with no appreciable effect on gene expression at a system-level has been challenging (19). Here, we have clustered mRNA targets by their correlation between mRNA abundance, transcriptome, and proteome in an effort to identify mRNAs that are post-transcriptionally regulated under steady-state conditions. We have applied this approach to identify functional targets of the small RNA *RsaO1* that is strongly upregulated by vancomycin in the clinical VISA isolate JKD6008.

Earlier work by Faigenbaum-Romm et al. (19) demonstrated that base-pairing strength (ΔG) is a poor predictor of functional sRNA targets from sRNA interactome data, and demonstrated a correlation between Hfq-binding, hybrid read count, and target repression (19). In *S. aureus*, most sRNAs appear to function independently of the small RNA chaperone Hfq leading to the suggestion that Hfq has been depreciated in *S. aureus* (53) and precluding this approach. We reasoned that post-transcriptional regulation may be reflected in a disconnect between mRNA and protein abundance under steady-state conditions. This is supported by the recent analysis of the *E. coli* transcriptome and proteome that demonstrates a strong correlation between mRNA and protein abundance (47). Indeed, these authors find that most of the genes that do not have a strong correlation are known to be post-transcriptionally regulated, including by small RNAs. Notably, this approach is likely to identify genes controlled by any mechanism of post-transcriptional regulation including through sequence features affecting translation efficiency such as codon usage, RNA secondary structures (e.g., RNA thermometers), RNA binding proteins, protein stability, as well as sRNA-mediated regulation (54–56).

SOMs were used to separate mRNAs into three clusters that have similar transcriptional and translational patterns. Cluster 1 appears to be translationally repressed in that genes have lower than expected protein abundance. Cluster 2 genes have transcript abundance that corresponded with protein expression, and genes in cluster 3 displayed slightly higher protein levels than transcript abundance potentially reflecting translation activation. Using sRNA-mRNA interactions that had previously been described and confirmed, 'verified interactions' were enriched in cluster 1 (lower protein levels). We find that CLASH interactions are recovered in all three clusters but are enriched in clusters 1 and 2. Cluster 2 RNA levels correspond to protein levels and for those functional sRNA-mRNA interactions in this cluster we interpret this as protein repression that is primarily driven by mRNA degradation.

Three sRNA-mRNA interactions from cluster 1 were validated using a GFP reporter assay and were found to be strongly repressive. The hybrid read position and predicted base-pairing indicated that these interactions occur around the RBS and start codon region of the target mRNA. To understand where sRNA-mRNA interactions occurred in all clusters, a metagene analysis of the RNase III-CLASH interactions in clusters 1–3 was performed and demonstrated enrichment around the 5' UTR and start codon in cluster 1 and to a lower degree in cluster 2 consistent with canonical repression through occlusion

of the 30S subunit. However, while cluster 1 contained many of the highest abundance hybrids, no statistically significant difference in mean hybrid counts between the three clusters was found which contrasts with earlier findings by Faigenbaum-Romm et al. (19). These results collectively suggest that cluster 1 contains functional sRNA-mRNA interactions that post-transcriptionally regulate mRNA translation.

Vancomycin intermediate *S. aureus* (VISA) is a major cause of vancomycin treatment failure. Many isolates have a thickened cell wall and reduced autolysis. Single nucleotide polymorphisms (SNPs) that confer the VISA phenotype can be heterogeneous and are poorly understood (2, 57–62). Previous analysis has suggested that small RNAs may contribute to the VISA phenotype (3). RsaOI (also termed sRNA131 and Sau6477) was the most upregulated sRNA in response to 8 µg/mL of vancomycin treatment in VISA, consistent with earlier work (3, 63), and was induced by vancomycin in a dose-dependent manner. RsaOI expression was not regulated by the vancomycin-responsive two-component system WalkR and we hypothesize that RsaOI is controlled by VraSR that is upregulated after vancomycin treatment and controls the divergent *vraABCP* operon (Fig. 6B).

To understand the function of RsaOI in *S. aureus*, we examined its mRNA targets. RsaOI has nine RNase III-CLASH mRNA targets and five of these are downregulated, suggesting that the RsaOI upregulation causes the repression of these five mRNA targets to adapt to antibiotic or cell wall stress. We repeated our SOMs clustering and included RNA-seq and proteomics data from VISA treated with 8 µg/mL vancomycin. RsaOI was earlier found to repress the expression of the RNase III-CLASH target *hpr* (phosphocarrier protein Hpr) which was detected in cluster 3 with the majority of experimentally characterised sRNA-mRNA interactions. The RsaOI target *atl* fell within cluster 1 and encodes for a bifunctional autolysin essential for cell wall turnover and cell division (50, 51). *Atl* has been previously implicated in glycopeptide intermediate resistance as it was found to be downregulated in several VISA strains relative to their respective VSSA parent strains. It was postulated that the downregulation of *atl* reduces autolytic activity and contributes to the thickened cell wall phenotype of VISA (1, 64, 65). In this study, we found that *atl* is downregulated in response to vancomycin in both the RNA-seq and proteomics data and it was present in cluster 1 of our vancomycin-treated SOMs analysis which display a pattern of corresponding transcript and protein levels. We demonstrated that RsaOI expression led to a 1.6-fold reduction in fluorescence signal in the *Atl*-GFP translation fusion and RNase III-CLASH predicted that RsaOI binds to the coding region of *atl* mRNA. This suggests that RsaOI forms a duplex with the *atl* mRNA that recruits RNase III for *atl* degradation and is consistent with mRNA decay driving reduced protein abundance (correlated mRNA/protein levels). As *atl* was found to be downregulated in several VISA isolates relative to VSSA parent strain (65), we reasoned that the knockdown of *atl* would result in increased growth in the presence of vancomycin. However, the *atl* CRISPRi knockdown had reduced growth without antibiotics and the growth defect was exacerbated by the addition of sub-MIC vancomycin. *Atl* functions in *S. aureus* cell division, where it forms a ring at the septum to facilitate partitioning of daughter cells (51, 66). It was previously reported that deleting *atl* causes a defect in daughter cell separation (67) and may explain the mutant phenotype.

Our data collectively suggest that RsaOI is an sRNA that is induced by vancomycin in VISA but is not required for vancomycin tolerance. A similar result was observed by reference (63), where deletion of several linezolid-induced differentially expressed sRNAs, including RsaOI, yielded no effect on the phenotype (63). *Atl* is also regulated by the sRNA, *SprC* (68), and potentially by the two-component regulatory system *SaeRS* (69) that may provide redundant layers of regulation. We speculate that RsaOI may be involved in a general cellular stress response (e.g., cell wall damage) that is not sufficient to resist vancomycin treatment and/or is functionally redundant.

The approach described here enabled the identification of post-transcriptionally regulated mRNAs and coupled with sRNA interactome data provide an initial step toward system-level functional characterization of the sRNA-mRNA interaction network. Using

these data, we have identified several targets of the vancomycin-responsive sRNA, RsaOI and demonstrated that one target, the cell wall autolysin *atl*, contributes to vancomycin tolerance. Our study suggests that the correlation between RNA and protein abundances at steady-state can be used to indicate the function of sRNA-mRNA pairs in sRNA interactome data.

ACKNOWLEDGMENTS

The authors thank Tim Stinear and Ian Monk for providing *S. aureus walkR* mutant strains. The authors also thank Peter Redder for insightful comments on the work.

W.W. was supported by an Australian Research Training Program scholarship. J.J.T., D.G.M., and W.W. are supported by grants from the National Health and Medical Research Council (NHMRC GNT1139313) and the Australian Research Council (ARC DP220101938).

AUTHOR AFFILIATIONS

¹School of Biotechnology and Biomolecular Sciences, Sydney, New South Wales, Australia

²Children's Medical Research Institute, Sydney, New South Wales, Australia

AUTHOR ORCIDs

Jai Justin Tree  <http://orcid.org/0000-0001-8233-0975>

FUNDING

Funder	Grant(s)	Author(s)
DHAC National Health and Medical Research Council (NHMRC)	GNT1139313	Jai Justin Tree
Department of Education and Training Australian Research Council (ARC)	DP220101938	Jai Justin Tree

AUTHOR CONTRIBUTIONS

Winton Wu, Investigation, Writing – original draft, Writing – review and editing | Chi Nam Ignatius Pang, Investigation | Daniel G. Mediati, Investigation | Jai Justin Tree, Supervision, Writing – original draft, Writing – review and editing

DATA AVAILABILITY

RNA sequencing data generated in this study are available at NCBI Gene Expression Omnibus (GEO; <https://www.ncbi.nlm.nih.gov/geo/>) under the SuperSeries accession number [GSE254533](https://www.ncbi.nlm.nih.gov/geo/query/acc.cgi?acc=GSE254533). Previously published *S. aureus* JKD6009 (VSSA) RNase III-CLASH data are available at NCBI GEO under the accession [GSE158830](https://www.ncbi.nlm.nih.gov/geo/query/acc.cgi?acc=GSE158830). The mass spectrometry proteomics data have been deposited to the ProteomeXchange Consortium via the PRIDE partner repository (<https://www.ebi.ac.uk/pride/>) with the data set identifier [PXD049022](https://www.ebi.ac.uk/pride/data/ebl-2023-01/PXD049022).

ADDITIONAL FILES

The following material is available [online](#).

Supplemental Material

Supplemental Figures (mSystems00971-23-S0001.pdf). Figures S1 to S7.

Table S1 (mSystems00971-23-S0002.xlsx). Strains and plasmids.

Table S2 (mSystems00971-23-S0003.xlsx). Oligonucleotides.

Table S3 (mSystems00971-23-S0004.xlsx). GO analysis.

Table S4 (mSystems00971-23-S0005.xlsx). Verified *S. aureus* sRNA-mRNA interactions overlaid with the SOMS clustering analysis.

REFERENCES

- Howden BP, McEvoy CRE, Allen DL, Chua K, Gao W, Harrison PF, Bell J, Coombs G, Bennett-Wood V, Porter JL, Robins-Browne R, Davies JK, Seemann T, Stinear TP. 2011. Evolution of multidrug resistance during *Staphylococcus aureus* infection involves mutation of the essential two component regulator WalkR. *PLoS Pathog* 7:e1002359. <https://doi.org/10.1371/journal.ppat.1002359>
- Howden BP, Davies JK, Johnson PDR, Stinear TP, Grayson ML. 2010. Reduced vancomycin susceptibility in *Staphylococcus aureus*, including vancomycin-intermediate and heterogeneous vancomycin-intermediate strains: resistance mechanisms, laboratory detection, and clinical implications. *Clin Microbiol Rev* 23:99–139. <https://doi.org/10.1128/CMR.00042-09>
- Howden BP, Beaume M, Harrison PF, Hernandez D, Schrenzel J, Seemann T, Francois P, Stinear TP. 2013. Analysis of the small RNA transcriptional response in multidrug-resistant *Staphylococcus aureus* after antimicrobial exposure. *Antimicrob Agents Chemother* 57:3864–3874. <https://doi.org/10.1128/AAC.00263-13>
- Bouvier M, Sharma CM, Mika F, Nierhaus KH, Vogel J. 2008. Small RNA binding to 5' mRNA coding region inhibits translational initiation. *Mol Cell* 32:827–837. <https://doi.org/10.1016/j.molcel.2008.10.027>
- Fröhlich KS, Vogel J. 2009. Activation of gene expression by small RNA. *Curr Opin Microbiol* 12:674–682. <https://doi.org/10.1016/j.mib.2009.09.009>
- Bandyra KJ, Said N, Pfeiffer V, Górna MW, Vogel J, Luisi BF. 2012. The seed region of a small RNA drives the controlled destruction of the target mRNA by the endoribonuclease RNase E. *Mol Cell* 47:943–953. <https://doi.org/10.1016/j.molcel.2012.07.015>
- Fröhlich KS, Papenfort K, Fekete A, Vogel J. 2013. A small RNA activates CFA synthase by isoform-specific mRNA stabilization. *EMBO J* 32:2963–2979. <https://doi.org/10.1038/emboj.2013.222>
- Sedlyarova N, Shamovsky I, Bharati BK, Epshtein V, Chen J, Gottesman S, Schroeder R, Nudler E. 2016. sRNA-mediated control of transcription termination in *E. coli*. *Cell* 167:111–121. <https://doi.org/10.1016/j.cell.2016.09.004>
- Jagodnik J, Chiaruttini C, Guillier M. 2017. Stem-loop structures within mRNA coding sequences activate translation initiation and mediate control by small regulatory RNAs. *Mol Cell* 68:158–170. <https://doi.org/10.1016/j.molcel.2017.08.015>
- Tree JJ, Granneman S, McAteer SP, Tollervey D, Gally DL. 2014. Identification of bacteriophage-encoded anti-sRNAs in pathogenic *Escherichia coli*. *Mol Cell* 55:199–213. <https://doi.org/10.1016/j.molcel.2014.05.006>
- Lalaoua D, Carrier M-C, Semsey S, Brouard J-S, Wang J, Wade JT, Massé E. 2015. A 3' external transcribed spacer in a tRNA transcript acts as a sponge for small RNAs to prevent transcriptional noise. *Mol Cell* 58:393–405. <https://doi.org/10.1016/j.molcel.2015.03.013>
- McKellar SW, Ivanova I, Arede P, Zapf RL, Mercier N, Chu L-C, Mediati DG, Pickering AC, Briaud P, Foster RG, Kudla G, Fitzgerald JR, Caldeleri I, Carroll RK, Tree JJ, Granneman S. 2022. RNase III CLASH in MRSA Uncovers sRNA regulatory networks coupling metabolism to toxin expression. *Nat Commun* 13:1–20. <https://doi.org/10.1038/s41467-022-31173-y>
- Waters SA, McAteer SP, Kudla G, Pang I, Deshpande NP, Amos TG, Leong KW, Wilkins MR, Strugnell R, Gally DL, Tollervey D, Tree JJ. 2017. Small RNA Interactome of pathogenic *E. coli* revealed through crosslinking of RNase E. *EMBO J* 36:374–387. <https://doi.org/10.15252/emboj.201694639>
- Iosub IA, van Nues RW, McKellar SW, Nieken KJ, Marchiorretto M, Sy B, Tree JJ, Viero G, Granneman S. 2020. Hfq CLASH uncovers sRNA-target interaction networks linked to nutrient availability adaptation. *Elife* 9:e54655. <https://doi.org/10.7554/eLife.54655>
- Matera G, Altuvia Y, Gerovac M, El Mouali Y, Margalit H, Vogel J. 2022. Global RNA Interactome of salmonella discovers a 5' UTR sponge for the MicF small RNA that connects membrane permeability to transport capacity. *Mol Cell* 82:629–644. <https://doi.org/10.1016/j.molcel.2021.12.030>
- Melamed S, Peer A, Faigenbaum-Romm R, Gatt YE, Reiss N, Bar A, Altuvia Y, Argaman L, Margalit H. 2016. Global mapping of small RNA-target interactions in bacteria. *Mol Cell* 63:884–897. <https://doi.org/10.1016/j.molcel.2016.07.026>
- Mediati DG, Wong JL, Gao W, McKellar S, Pang CNI, Wu S, Wu W, Sy B, Monk IR, Biazik JM, Wilkins MR, Howden BP, Stinear TP, Granneman S, Tree JJ. 2022. RNase III-CLASH of multi-drug resistant *Staphylococcus aureus* reveals a regulatory mRNA 3' UTR required for intermediate vancomycin resistance. *Nat Commun* 13:1–15. <https://doi.org/10.1038/s41467-022-31177-8>
- Liu F, Chen Z, Zhang S, Wu K, Bei C, Wang C, Chao Y. 2023. *In vivo* RNA Interactome profiling reveals 3'UTR-processed small RNA targeting a central regulatory hub. *Nat Commun* 14:8106. <https://doi.org/10.1038/s41467-023-43632-1>
- Faigenbaum-Romm R, Reich A, Gatt YE, Barsheset M, Argaman L, Margalit H. 2020. Hierarchy in Hfq chaperon occupancy of small RNA targets plays a major role in their regulation. *Cell Rep* 30:3127–3138. <https://doi.org/10.1016/j.celrep.2020.02.016>
- Zhang W, Wang J, Jin D, Oreopoulos L, Zhang Z. 2018. “A deterministic self-organizing map approach and its application on satellite data based cloud type classification” 2018 IEEE International Conference on Big Data (Big Data); Seattle, WA, USA: , p 2027–2034. <https://doi.org/10.1109/BigData.2018.8622558>
- Kiang MY. 2001. Extending the Kohonen self-organizing map networks for clustering analysis. *Computational Statistics & Data Analysis* 38:161–180. [https://doi.org/10.1016/S0167-9473\(01\)00040-8](https://doi.org/10.1016/S0167-9473(01)00040-8)
- Mortazavi A, Pepke S, Jansen C, Marinov GK, Ernst J, Kellis M, Hardison RC, Myers RM, Wold BJ. 2013. Integrating and mining the chromatin landscape of cell-type specificity using self-organizing maps. *Genome Res* 23:2136–2148. <https://doi.org/10.1101/gr.158261.113>
- Moorman C, Sun LV, Wang J, de Wit E, Talhout W, Ward LD, Greil F, Lu X-J, White KP, Bussemaker HJ, van Steensel B. 2006. Hotspots of transcription factor colocalization in the genome of *Drosophila melanogaster*. *Proc Natl Acad Sci USA* 103:12027–12032. <https://doi.org/10.1073/pnas.0605003103>
- Spencer WC, Zeller G, Watson JD, Henz SR, Watkins KL, McWhirter RD, Petersen S, Sreedharan VT, Widmer C, Jo J, Reinke V, Petrella L, Strome S, Von Stetina SE, Katz M, Shaham S, Ratsch G, Miller DM. 2011. A spatial and temporal map of *C. elegans* gene expression. *Genome Res* 21:325–341. <https://doi.org/10.1101/gr.114595.110>
- Golub TR, Slonim DK, Tamayo P, Huard C, Gaasenbeek M, Mesirov JP, Coller H, Loh ML, Downing JR, Caligiuri MA, Bloomfield CD, Lander ES. 1999. Molecular classification of cancer: class discovery and class prediction by gene expression monitoring. *Science* 286:531–537. <https://doi.org/10.1126/science.286.5439.531>
- Milone DH, Stegmayer GS, Kamenetzky L, López M, Lee JM, Giovannoni JJ, Carrari F. 2010. romeSOM: a software for clustering and visualization of transcriptional and metabolite data mined from interspecific crosses of crop plants. *BMC Bioinformatics* 11:438. <https://doi.org/10.1186/1471-2105-11-438>
- Tamayo P, Slonim D, Mesirov J, Zhu Q, Kitareewan S, Dmitrovsky E, Lander ES, Golub TR. 1999. Interpreting patterns of gene expression with self-organizing maps: methods and application to hematopoietic differentiation. *Proc Natl Acad Sci USA* 96:2907–2912. <https://doi.org/10.1073/pnas.96.6.2907>
- Weber M, Teeling H, Huang S, Waldmann J, Kassabgy M, Fuchs BM, Klindworth A, Klockow C, Wichels A, Gerds G, Amann R, Glöckner FO. 2011. Practical application of self-organizing maps to interrelate Biodiversity and functional data in NGS-based metagenomics. *ISME J* 5:918–928. <https://doi.org/10.1038/ismej.2010.180>
- Abe T, Akazawa Y, Toyoda A, Niki H, Baba T. 2020. Batch-learning self-organizing map identifies horizontal gene transfer candidates and their origins in entire genomes. *Front Microbiol* 11:1486. <https://doi.org/10.3389/fmicb.2020.01486>
- Monk IR, Shah IM, Xu M, Tan MW, Foster TJ. 2012. Transforming the untransformable: application of direct transcription to manipulate genetically *Staphylococcus aureus* and *Staphylococcus epidermidis*. *mBio* 3:e00277-11. <https://doi.org/10.1128/mBio.00277-11>
- Otto TD, Dillon GP, Degraeve WS, Berriman M. 2011. RATT: rapid annotation transfer tool. *Nucleic Acids Res* 39:e57. <https://doi.org/10.1093/nar/gkq1268>
- Bushnell B. 2014. Bbtools software package. Available from: <http://sourceforge.net/projects/bbmap>

33. Bushnell B, Rood J, Singer E. 2017. BBMerge—accurate paired shotgun read merging via overlap. *PLoS One* 12:e0185056. <https://doi.org/10.1371/journal.pone.0185056>
34. Love MI, Huber W, Anders S. 2014. Moderated estimation of fold change and dispersion for RNA-seq data with DESeq2. *Genome Biol* 15:550. <https://doi.org/10.1186/s13059-014-0550-8>
35. Latif H, Szubin R, Tan J, Brunk E, Lechner A, Zengler K, Palsson BO. 2015. A streamlined ribosome profiling protocol for the characterization of microorganisms. *Biotechniques* 58:329–332. <https://doi.org/10.2144/000114302>
36. Choe D, Lee JH, Yoo M, Hwang S, Sung BH, Cho S, Palsson B, Kim SC, Cho B-K. 2019. Adaptive laboratory evolution of a genome-reduced *Escherichia coli*. *Nat Commun* 10:1–14. <https://doi.org/10.1038/s41467-019-08888-6>
37. Oh E, Becker AH, Sandikci A, Huber D, Chaba R, Gloge F, Nichols RJ, Typas A, Gross CA, Kramer G, Weissman JS, Bukau B. 2011. Selective ribosome profiling reveals the cotranslational chaperone action of trigger factor *in vivo*. *Cell* 147:1295–1308. <https://doi.org/10.1016/j.cell.2011.10.044>
38. Cox J, Mann M. 2008. MaxQuant enables high peptide identification rates, individualized ppp-range mass accuracies and proteome-wide protein quantification. *Nat Biotechnol* 26:1367–1372. <https://doi.org/10.1038/nbt.1511>
39. The UniProt Consortium. 2007. The universal protein resource (UniProt). *Nucleic acids research*:D190–D195. <https://doi.org/10.1093/nar/gkm895>
40. Tyanova S, Temu T, Sinitcyn P, Carlson A, Hein MY, Geiger T, Mann M, Cox J. 2016. The perseus computational platform for comprehensive analysis of (prote) omics data. *Nat Methods* 13:731–740. <https://doi.org/10.1038/nmeth.3901>
41. Wehrens R, Buydens LM. 2007. Self-and super-organizing maps in R: the kohonen package. *J Stat Softw* 21:1–19. <https://doi.org/10.18637/jss.v021.i05>
42. Ivain L, Bordeau V, Eyraud A, Hallier M, Dreano S, Tattevin P, Felden B, Chabelskaya S. 2017. An *in vivo* reporter assay for sRNA-directed gene control in gram-positive bacteria: identifying a novel sRNA target in *Staphylococcus aureus*. *Nucleic Acids Res* 45:4994–5007. <https://doi.org/10.1093/nar/gkx190>
43. Webb S, Hector RD, Kudla G, Granneman S. 2014. PAR-CLIP data indicate that Nrd1-Nab3-dependent transcription termination regulates expression of hundreds of protein coding genes in yeast. *Genome Biol* 15:R8. <https://doi.org/10.1186/gb-2014-15-1-r8>
44. Travis AJ, Moody J, Helwak A, Tollervey D, Kudla G. 2014. Hyb: a bioinformatics pipeline for the analysis of CLASH (Crosslinking, ligation and sequencing of hybrids) data. *Methods* 65:263–273. <https://doi.org/10.1016/j.ymeth.2013.10.015>
45. Eyraud A, Tattevin P, Chabelskaya S, Felden B. 2014. A small RNA controls a protein regulator involved in antibiotic resistance in *Staphylococcus aureus*. *Nucleic Acids Res* 42:4892–4905. <https://doi.org/10.1093/nar/gku149>
46. Tomasini A, Moreau K, Chicher J, Geissmann T, Vandenesch F, Romby P, Marzi S, Caldelari I. 2017. The RNA targetome of *Staphylococcus aureus* non-coding RNA RsaA: impact on cell surface properties and defense mechanisms. *Nucleic Acids Res* 45:6746–6760. <https://doi.org/10.1093/nar/gkx219>
47. Balakrishnan R, Mori M, Segota I, Zhang Z, Aebersold R, Ludwig C, Hwa T. 2022. Principles of gene regulation quantitatively connect DNA to RNA and proteins in bacteria. *Science* 378:eabk2066. <https://doi.org/10.1126/science.abk2066>
48. Kohonen T. 2013. Essentials of the self-organizing map. *Neural Netw* 37:52–65. <https://doi.org/10.1016/j.neunet.2012.09.018>
49. Bohn C, Rigoulay C, Chabelskaya S, Sharma CM, Marchais A, Skorski P, Borezée-Durant E, Barbet R, Jacquet E, Jacq A, Gautheret D, Felden B, Vogel J, Boulou P. 2010. Experimental discovery of small RNAs in *Staphylococcus aureus* reveals a riboregulator of central metabolism. *Nucleic Acids Res* 38:6620–6636. <https://doi.org/10.1093/nar/gkq462>
50. Zheng X, Ma SX, St John A, Torres VJ. 2022. The major autolysin Atl regulates the virulence of *Staphylococcus aureus* by controlling the sorting of LukAB. *Infect Immun* 90:e0005622. <https://doi.org/10.1128/iai.00056-22>
51. Nega M, Tribelli PM, Hipp K, Stahl M, Götz F. 2020. New insights in the coordinated amidase and glucosaminidase activity of the major autolysin (Atl) in *Staphylococcus aureus*. *Commun Biol* 3:1–10. <https://doi.org/10.1038/s42003-020-01405-2>
52. Zhang YF, Han K, Chandler CE, Tjaden B, Ernst RK, Lory S. 2017. Probing the sRNA regulatory landscape of *P. aeruginosa*: post-transcriptional control of determinants of pathogenicity and antibiotic susceptibility. *Mol Microbiol* 106:919–937. <https://doi.org/10.1111/mmi.13857>
53. Bohn C, Rigoulay C, Boulou P. 2007. No detectable effect of RNA-binding protein Hfq absence in *Staphylococcus aureus*. *BMC Microbiol* 7:10. <https://doi.org/10.1186/1471-2180-7-10>
54. Nie L, Wu G, Zhang W. 2006. Correlation of mRNA expression and protein abundance affected by multiple sequence features related to translational efficiency in *Desulfovibrio vulgaris*: a quantitative analysis. *Genetics* 174:2229–2243. <https://doi.org/10.1534/genetics.106.065862>
55. Maier T, Güell M, Serrano L. 2009. Correlation of mRNA and protein in complex biological samples. *FEBS Lett* 583:3966–3973. <https://doi.org/10.1016/j.febslet.2009.10.036>
56. Van Assche E, Van Puyvelde S, Vanderleyden J, Steenackers HP. 2015. RNA-binding proteins involved in post-transcriptional regulation in bacteria. *Front Microbiol* 6:141. <https://doi.org/10.3389/fmicb.2015.00141>
57. Mwangi MM, Wu SW, Zhou Y, Sieradzki K, de Lencastre H, Richardson P, Bruce D, Rubin E, Myers E, Siggia ED, Tomasz A. 2007. Tracking the *in vivo* evolution of multidrug resistance in *Staphylococcus aureus* by whole-genome sequencing. *Proc Natl Acad Sci USA* 104:9451–9456. <https://doi.org/10.1073/pnas.0609839104>
58. Scherl A, François P, Charbonnier Y, Deshusses JM, Koessler T, Huyghe A, Bento M, Stahl-Zeng J, Fischer A, Masselot A, Vaezzadeh A, Gallé F, Renzoni A, Vaudaux P, Lew D, Zimmermann-Ivol CG, Binz P-A, Sanchez J-C, Hochstrasser DF, Schrenzel J. 2006. Exploring glycopeptide-resistance in *Staphylococcus aureus*: a combined Proteomics and Transcriptomics approach for the identification of resistance-related markers. *BMC Genomics* 7:296. <https://doi.org/10.1186/1471-2164-7-296>
59. Peltz RF, Singh VK, Schmidt JL, Batten MA, Baranyak CS, Nadakavukaren MJ, Jayaswal RK, Wilkinson BJ. 2000. Characterization of passage-selected vancomycin-resistant *Staphylococcus aureus* strains of diverse parental backgrounds. *Antimicrob Agents Chemother* 44:294–303. <https://doi.org/10.1128/AAC.44.2.294-303.2000>
60. Muthaiyan A, Jayaswal RK, Wilkinson BJ. 2004. Intact *mutS* in laboratory-derived and clinical glycopeptide-intermediate *Staphylococcus aureus* strains. *Antimicrob Agents Chemother* 48:623–625. <https://doi.org/10.1128/AAC.48.2.623-625.2004>
61. Cui L, Ma X, Sato K, Okuma K, Tenover FC, Mamizuka EM, Gemmell CG, Kim MN, Ploy MC, El-Sohl N, Ferraz V, Hiramatsu K. 2003. Cell wall thickening is a common feature of vancomycin resistance in *Staphylococcus aureus*. *J Clin Microbiol* 41:5–14. <https://doi.org/10.1128/JCM.41.1.5-14.2003>
62. Renzoni A, Barras C, François P, Charbonnier Y, Huggler E, Garzoni C, Kelley WL, Majcherczyk P, Schrenzel J, Lew DP, Vaudaux P. 2006. Transcriptomic and functional analysis of an autolysin-deficient, teicoplanin-resistant derivative of methicillin-resistant *Staphylococcus aureus*. *Antimicrob Agents Chemother* 50:3048–3061. <https://doi.org/10.1128/AAC.00113-06>
63. Gao W, Guérillot R, Lin YH, Tree J, Beaume M, François P, Monk IR, Seemann T, Schrenzel J, Howden BP, Stinear TP. 2020. Comparative transcriptomic and functional assessments of linezolid-responsive small RNA genes in *Staphylococcus aureus*. *mSystems* 5:e00665-19. <https://doi.org/10.1128/mSystems.00665-19>
64. Cafso V, Bertuccio T, Spina D, Purrello S, Campanile F, Di Pietro C, Purrello M, Stefani S. 2012. Modulating activity of vancomycin and daptomycin on the expression of autolysin cell-wall turnover and membrane charge genes in hVISA and VISA strains. *PLoS One* 7:e29573. <https://doi.org/10.1371/journal.pone.0029573>
65. Wootton M, Bennett PM, MacGowan AP, Walsh TR. 2005. Reduced expression of the ATL Autolysin gene and susceptibility to autolysin in clinical heterogeneous glycopeptide-intermediate *Staphylococcus aureus* (hGISA) and GISA strains. *J Antimicrob Chemother* 56:944–947. <https://doi.org/10.1093/jac/dki289>
66. Yamada S, Sugai M, Komatsuzawa H, Nakashima S, Oshida T, Matsumoto A, Suginaka H. 1996. An Autolysin ring associated with cell separation of *Staphylococcus aureus*. *J Bacteriol* 178:1565–1571. <https://doi.org/10.1128/jb.178.6.1565-1571.1996>

67. Bose JL, Lehman MK, Fey PD, Bayles KW. 2012. Contribution of the *Staphylococcus aureus* Atl AM and GL murein hydrolase activities in cell division, autolysis, and biofilm formation. PLoS One 7:e42244. <https://doi.org/10.1371/journal.pone.0042244>
68. Le Pabic H, Germain-Amiot N, Bordeau V, Felden B. 2015. A bacterial regulatory RNA attenuates virulence, spread and human host cell phagocytosis. Nucleic Acids Res 43:9232–9248. <https://doi.org/10.1093/nar/gkv783>
69. Cue D, Junecko JM, Lei MG, Blevins JS, Smeltzer MS, Lee CY. 2015. SaeRS-dependent inhibition of biofilm formation in *Staphylococcus aureus* Newman. PLoS One 10:e0123027. <https://doi.org/10.1371/journal.pone.0123027>